環境変動の記録媒体とその磁気的情報：堆積物

深海底堆積物コア

Kent (1982)
南インド洋
(48.5°S, 79.9°E)

酸素同位対比と
帯磁率の相関

寒冷期：
強磁性鉱物の供給多
炭酸カルシウム量少
（希釈効果小）

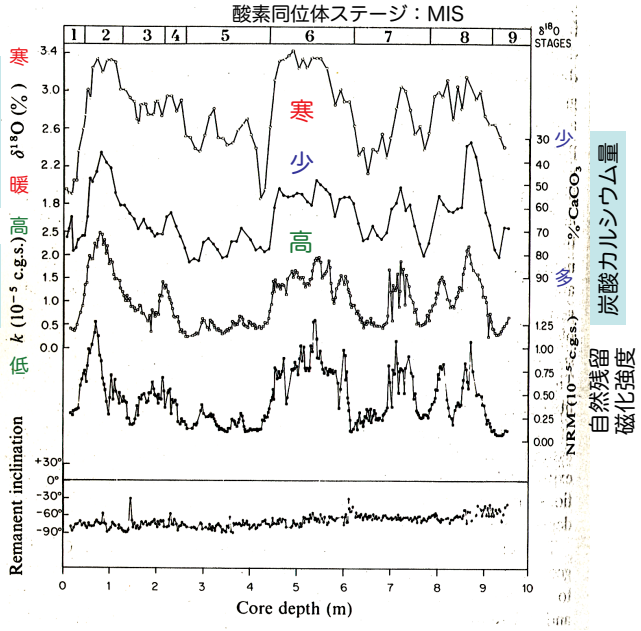

深海底コア：帯磁率ーモンスーン変動

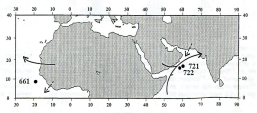

帯磁率変動に周期性
10万年，4.1万年
2.3万年，1.9万年

“ミランコヴィッチ周期”

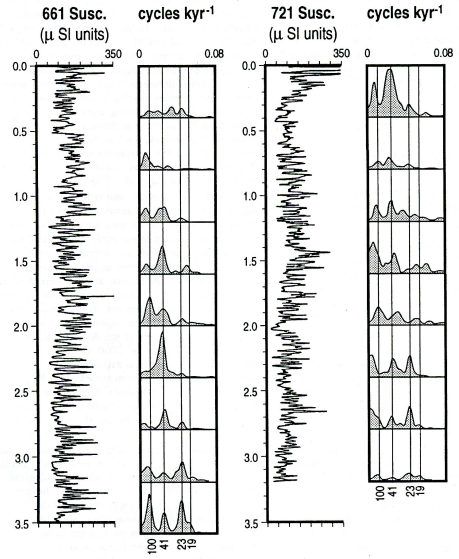

中緯度大西洋

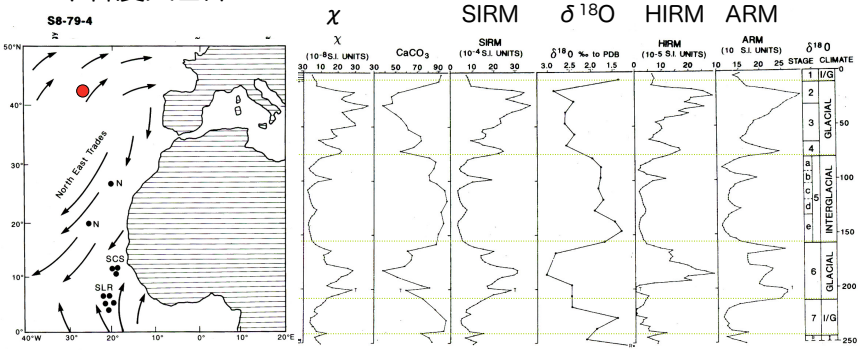

Figure 4.2. Magnetic properties of core S8-79-4, together with its late Pleistocene record of $\delta^{18}O$, carbonate content and planktic foraminifera (reprinted from *Phys. Earth Planet. Int.*, **42**, Robinson, 'The late Pleistocene palaeoclimatic record of North Atlantic deep-sea sediments revealed by mineral-magnetic measurements', 22–47, Copyright 1986, with permission from Elsevier Science).

χ,SIRM：強磁性鉱物の量
ARM：マグネタイトの量（細粒）
HIRM：高保磁力粒子の量
（ヘマタイト，ゲータイト）

- $\delta^{18}O$と良い相関
- 氷期：
  各パラメータ増加（強磁性鉱物量の増加）
  HIRM → 高保磁力粒子の増加

＊風成塵の増加
陸域の拡大・乾燥，風速の増大

中緯度大西洋

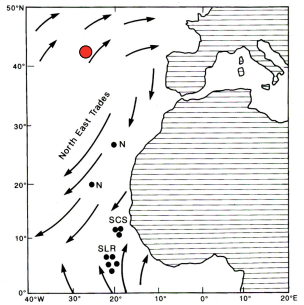

高保磁力粒子の寄与　　マグネタイトの粒子サイズ

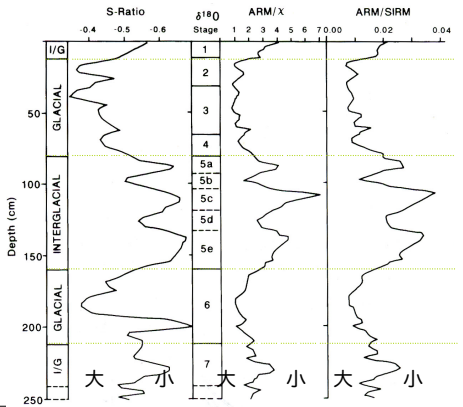

S-ratio：IRM(0.3T)/SIRM
高保磁力粒子の寄与
（ヘマタイト，ゲータイト）
ARM/χ，ARM/SIRM：
マグネタイトの粒子サイズ

氷期：
S-ratio →高保磁力粒子の増加
間氷期：
細粒マグネタイトの増加

Yancheva et al. (Nature, 2007)
Influence of the intertropical convergence zone on the East Asian monsoon

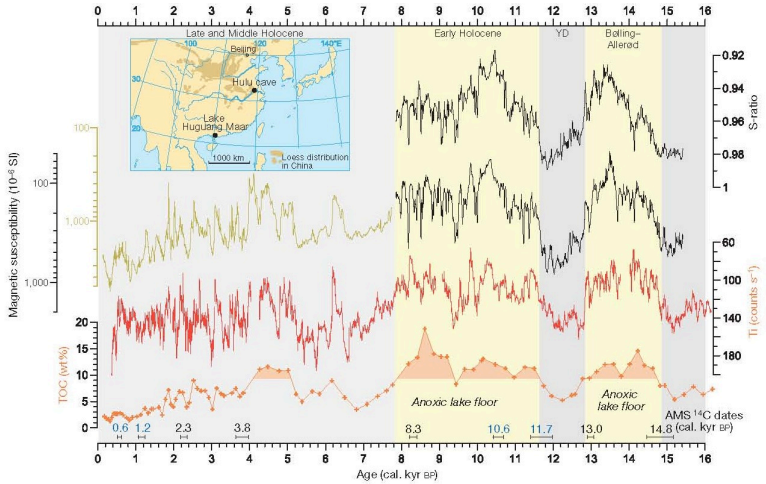

Figure 1 | Palaeoclimate time series of Lake Huguang Maar. Rock magnetic parameters (magnetic susceptibility and S-ratio), and Ti and TOC content from the sediment sequence during the past 16 kyr. Distinct intervals of anoxic conditions at the lake bottom are shaded in yellow. The S-ratio is saturated at 1 after 7.8 kyr BP. Five AMS ^{14}C dates of leaves (black) and four of bulk sediment (blue) are shown with an uncertainty interval of 2σ. Inset, locations of Lake Huguang Maar, Hulu cave and the Chinese loess plateau.

Yancheva et al. (Nature, 2007)
Influence of the intertropical convergence zone on the East Asian monsoon

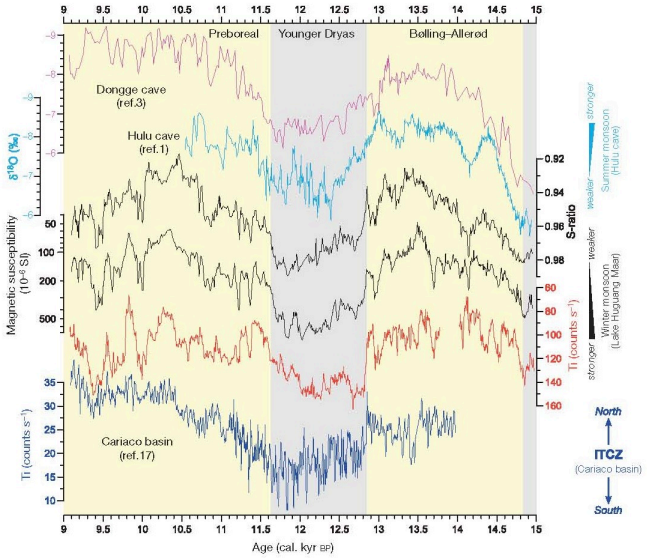

Figure 2 | Comparison of the monsoon sensitive sedimentary records from Lake Huguang Maar with other climate records. These are from the Cariaco basin[17], in the southern Caribbean off Venezuela, and Hulu and Dongge caves[1–3]. The Bølling-Allerød, Younger Dryas and Preboreal are highlighted.

琵琶湖コア

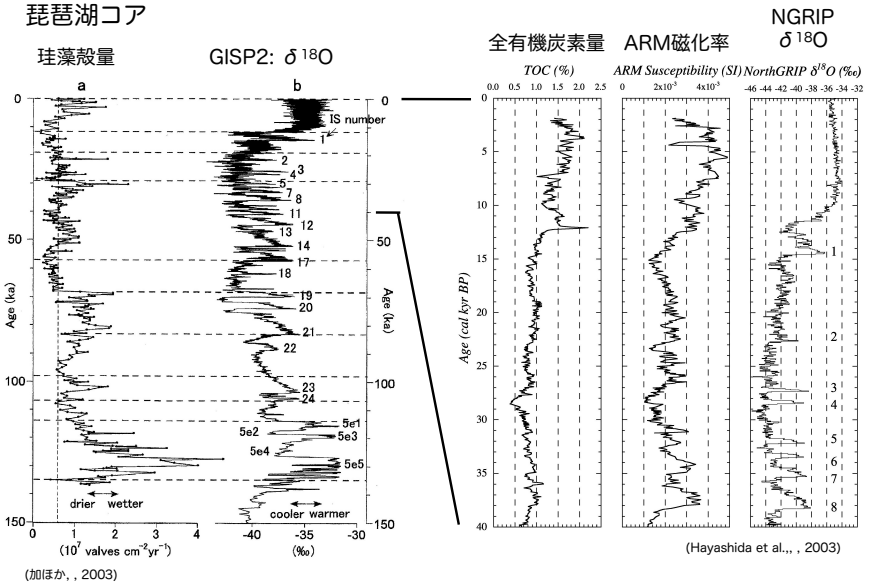

ダンスガード・オシュガー・サイクル（Dansgaard-Oeschger cycle）

レス：風成層
石英，斜長石が主

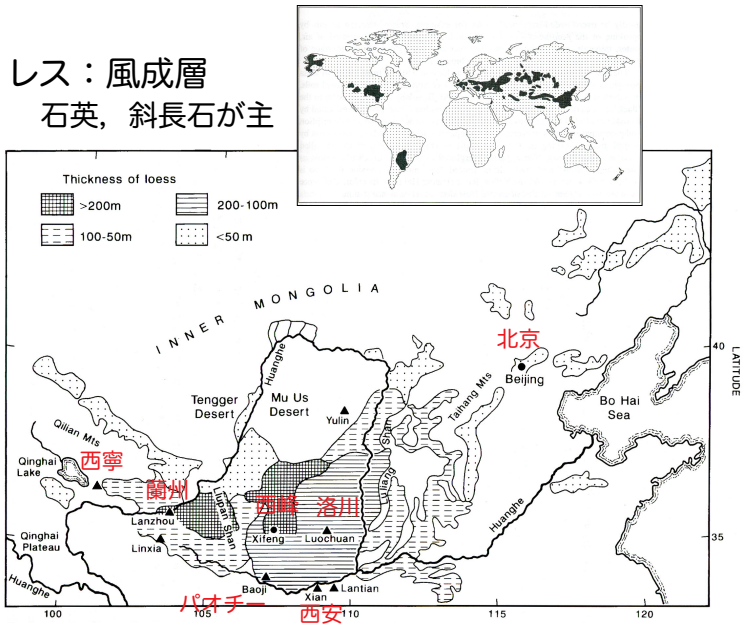

赤道太平洋
深海底堆積物

黄土層

レス（黄土）と
古土壌の互層

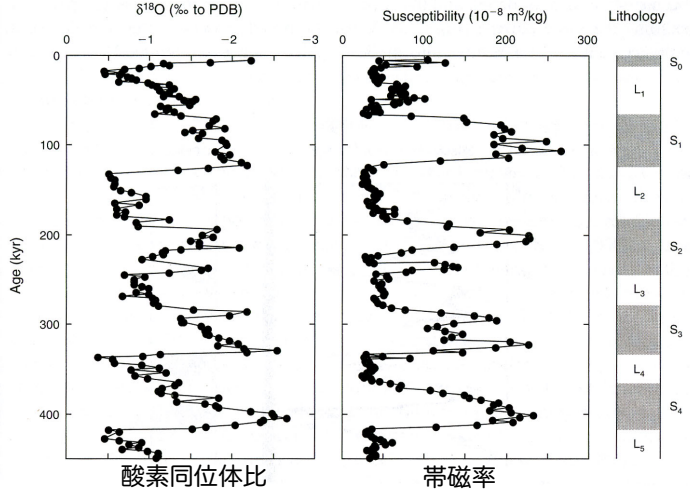

レス：寒冷期
帯磁率低

古土壌：温暖期
帯磁率高

帯磁率変動
の解釈
↓
土壌化モデル

＊土壌化モデル：土壌化による強磁性鉱物（マグネタイト，マグヘマイト）の形成

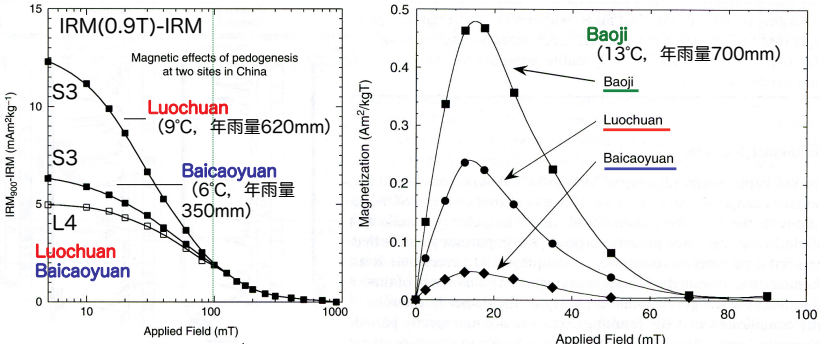

100mT以下でIRMを
獲得する鉱物の量
レス (L4) ＜古土壌 (S3)
＊より温暖・湿潤な地域
ほどその量は多い

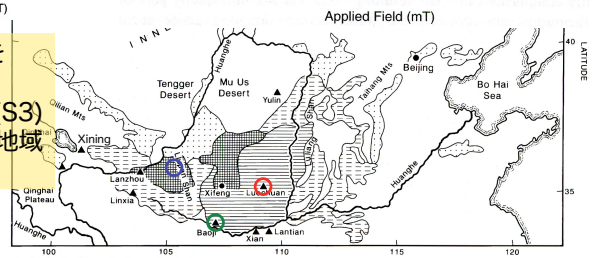

(Evans & Heller, 200

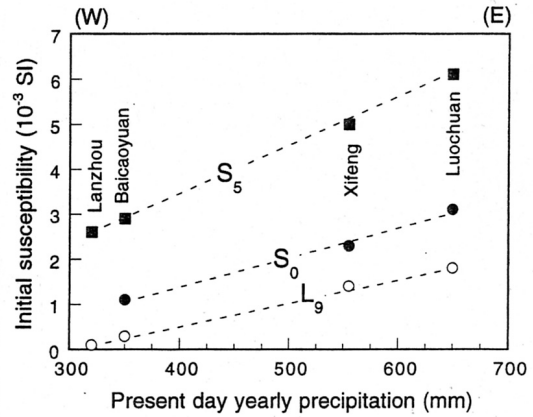

図 6　黄土高原の蘭州 (Lanzhou)，白草塬 (Baicaoyuan)，西峰 (Xifeng)，洛川 (Luochuan) での現在の降水量と黄土層の初磁化率との関係
Heller *et al.* (1993) を一部簡略化．（鳥居・福間, 1998）

黄土層の帯磁率と現在の降水量に正の相関

黄土高原の現在の土壌の帯磁率と
年間降雨量の関係

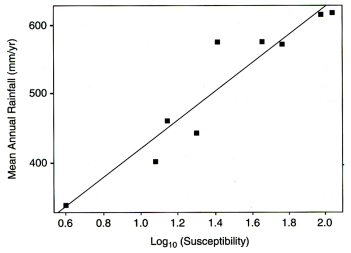

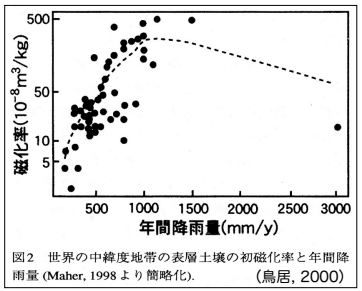

図2　世界の中緯度地帯の表層土壌の初磁化率と年間降雨量 (Maher, 1998 より簡略化).　（鳥居, 2000）

帯磁率から推定した年間降雨量（現在との差）

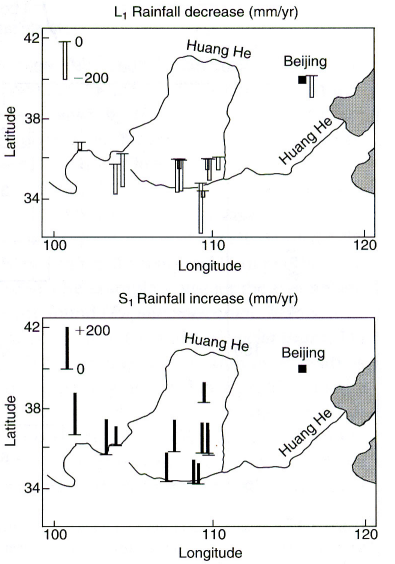

(Evans & Heller, 2003)

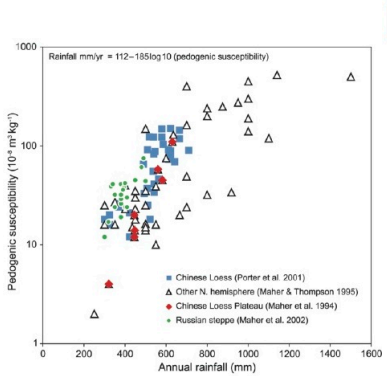

FIGURE 5 Relationship between pedogenic (soil-formed) magnetic susceptibility and annual rainfall for modern loessic soils and modern (last 30-year averages) rainfall. Statistical examination of the relationships between the soil magnetic properties and major climate variables (temperature, rainfall, etc.) identifies annual rainfall as the most significant factor ($R^2 = 0.88$). The relationship between soil magnetism and rainfall can thus be expressed as the equation shown in the figure. FROM MAHER ET AL. 2002

(Maher: Elements, 2009)

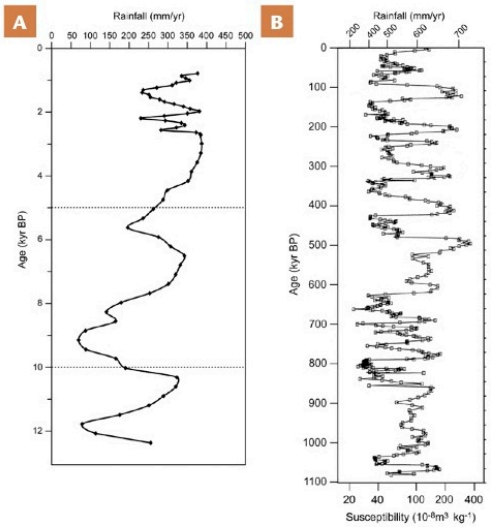

FIGURE 6 Palaeorainfall estimated from the magnetic susceptibility/rainfall climofunction for (**A**) the last 10,000 years (Duowa, western Loess Plateau) and (**B**) the last 1.1 million years (Xifeng, central Plateau). FROM MAHER AND THOMPSON (1995) AND MAHER (2008)

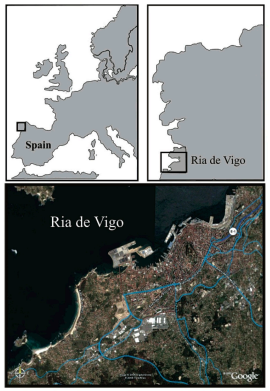

FIGURE 1. Top: Location of the area of study in northwest Spain. Bottom: Satellite picture of the area of study equivalent to map shown in Figure 2. Blue lines indicate main traffic axes (courtesy of http://earth.google.com/).

Devila et al. (Environ. Sci. Technol. 2006)
Mapping the Sources of Urban Dust in a Coastal Environment by Measuring Magnetic Parameters of Platanus hispanica Leaves

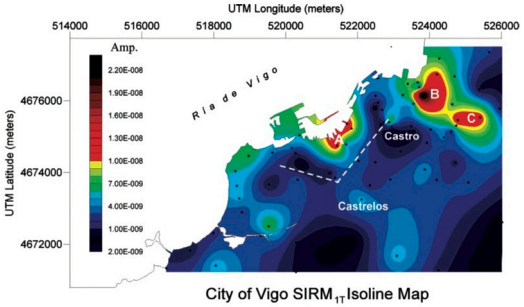

FIGURE 2. Map distribution of the SIRM$_{1T}$ over the area of study. Overall, samples from the urban area yielded larger values than those from the suburban area. The three maximums (labeled A, B, and C) coincide with main traffic axes and with shipyard and harbor activities. The city's topographic maximum height (dashed line) influences the distribution of magnetic PM. Minimum values are related to the two urban parks (Castro and Castrelos) and to noninhabited areas of the in the southeastern outskirts of the city.

Devila et al. (2006)

TABLE 2. Heavy Metal Concentration of 8 Representative Samples with High (Top) and Low (Bottom) Sirm$_{1T}$ Values[a]

	Cr (ppb/m^2)	Cu (ppb/m^2)	Fe (ppb/m^2)	Mn (ppb/m^2)	Ni (ppb/m^2)	Pb (ppb/m^2)	Zn (ppb/m^2)	Σ heavy metal	SIRM$_{1T}$ (A)
5	137	593	10 892	1,443	60	93	2353	15 571	1.12×10^{-8}
22	307	1508	13 602	4,020	162	255	6205	26 059	2.24×10^{-8}
27	72	573	7702	1803	60	125	2672	13 007	8.00×10^{-9}
72	1,002	4842	4752	4,703	28	68	1475	16 870	1.08×10^{-8}
73	60	638	8458	1587	55	168	2937	13 903	1.01×10^{-8}
	315.6	**1630.8**	**9081.2**	**2711.2**	**73**	**141.8**	**3128.4**		**1.25×10^{-8}**
15	1172	275	765	6070	55	13	1722	10 072	1.07×10^{-9}
59	97	350	253	668	22	10	923	2323	9.84×10^{-10}
74	145	403	912	4837	50	10	928	7285	4.17×10^{-10}
	471.3	**342.66**	**643.3**	**3858.33**	**43.3**	**11**	**1191**		**8.25×10^{-10}**

[a] Numbers in bold indicate mean values.

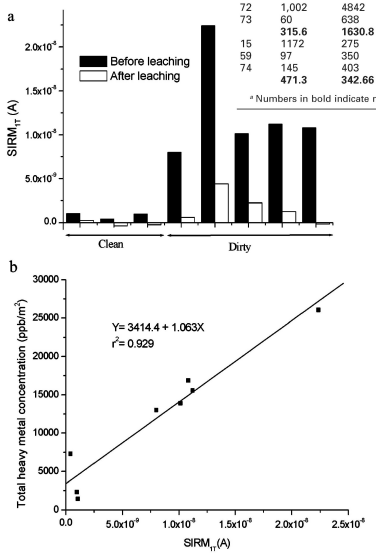

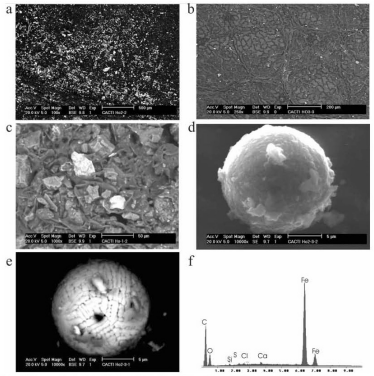

FIGURE 4. (a) SEM micrograph of a leaf with large SIRM$_{1T}$ signal (referred to as dirty throughout the text), with a large amount of urban PM. Scale bar is 500 μm. (b) SEM micrograph of a leaf with low SIRM$_{1T}$ signal (referred to as clean throughout the text), with a low amount of urban PM. Scale bar is 200 μm. (c) Larger, iron-bearing particle associated to the erosion of terrigenous materials as well as to alteration of urban structures (pavements, building facades, etc.), and also responsible for the magnetic signal of the leaves. Scale bar is 50μm. (d) and (e) Flying ashes responsible for the magnetic signal of the leaves, the size of these spherules (~18 μm) makes them particularly hazardous to public health. Scale bars are 5 μm. (f) EDXRA analysis of the flying ashes which reveals iron and oxygen as the main elements.

Mahera et al.
(Atmospheric Environment, 2008)

Spatial variation in vehicle-derived metal pollution identified by magnetic and elemental analysis of roadside tree leaves

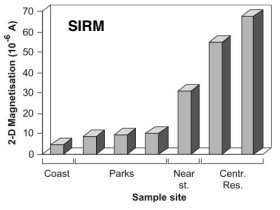

Fig. 1. Variation with location of 2-D magnetic remanence values (SIRMs), measured on sampled birch leaves, from Weybourne on the Norfolk coast to the central reservation of Grapes Hill, a major city centre dual carriageway.

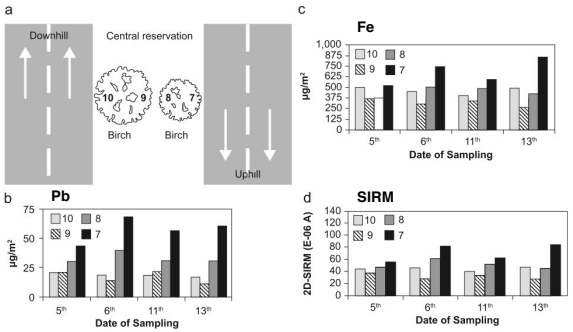

Fig. 2. Pb, Fe and 2-D SIRM values for tree leaves sampled across the central reservation of the uphill and downhill lanes of a major dual carriageway (Grapes Hill) in Norwich, UK: (a) sample locations, (b) Pb concentrations, (c) Fe concentrations, (d) 2-D SIRM. Leaves were sampled over a predominantly dry summer period (5–13/08/1999); heavy rain fell overnight between 06/08/1999 and 11/08/1999.

a

	SIRM	Fe	Pb	Zn	Mn	Ba
SIRM	1					
Fe	0.976	1				
Pb	0.871	0.849	1			
Zn	0.035	0.028	0.101	1		
Mn	0.009	0.014	0.014	0.444	1	
Ba	0.001	0.006	0.003	0.414	0.500	1

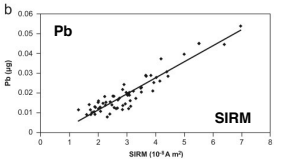

Fig. 3. Correlations between leaf particulate metal concentrations and SIRM, Grapes Hill, Norwich: (a) all analysed metals ($n = 40$, shaded boxes with significance <0.05) and (b) Pb concentration and SIRM ($n = 40$, $p \leq 0.0005$).

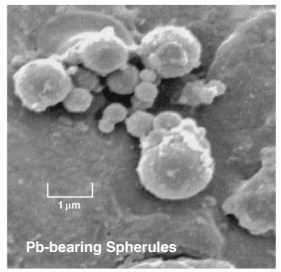

Fig. 5. Scanning electron micrograph of clustered, spherical leaf particulates, Grapes Hill, Norwich. From EDXA analysis, Pb occurs (as a minor element) only within the spherules <1 μm diameter.